RESEARCH PAPER

Influence of weld geometry and residual stresses on the fatigue strength of longitudinal stiffeners

J. Baumgartner · T. Bruder

Abstract Typically, for a fatigue strength assessment of a welded structure, the influence of welding residual stresses has to be considered. An easy applicable approach is given within the framework of the IIW recommendations; the design S-N curves can be upgraded in case of medium or low residual stresses. A relaxation or redistribution of tensile residual stresses, which is often accompanied by an increase in fatigue life, cannot be considered. To obtain a better understanding of the residual stresses and their influence on the fatigue strength, fatigue tests have been performed on longitudinal stiffeners in as-welded and stress relieved state with both stress ratios $R=-1$ and $R=0$. Local strains and stresses were measured using strain gauges and X-ray diffraction technique to get insight into the local material's response due to global loading close to the weld toe. The crack initiation and propagation phase was detected by a camera. FE models were set up to reproduce the observed material behavior in the notch for the crack initiation phase. By numerical analysis it could be shown that, due to sharp notches at the weld toe with an average toe radius of $r=0.05$ mm, a stress redistribution occurs during the first load cycle. This leads to a fatigue strength, which is, particularly at higher load amplitudes, independent from mean as well as from initial residual stresses. A comparison of fatigue data derived on longitudinal stiffeners from literature confirms this effect. For lower load amplitudes instead, mean and residual stresses gain more influence. In this investigation a reliable assessment of the crack initiation period could be performed with strain-based concepts using damage parameter P_{SWT} for a mean stress assessment. All fatigue tests could be transformed into a single damage parameter P_{SWT}-N curve with a low scatter if residual stresses as well as the distortion of the specimens are regarded.

1 Introduction

For many decades the influence of residual stresses on the fatigue strength was subject of investigation in numerous research projects, i.e. [13, 24, 37, 39]. In many of these projects an increase in fatigue strength could be observed if specimens were stress relieve heat treated. Two different effects could be observed: In some investigations the heat treatment lead to a shift towards shallower S-N curves, in others the knee point seemed to shift towards a lower number of cycles.

In more recent projects the development of residual stresses at welded specimens due to cyclic loading was measured using neutron or X-ray diffraction technique [6, 12, 18, 21, 28]. In those investigations a change in residual stresses was measured, which was more pronounced at high load amplitudes. For the majority of specimens a relaxation of the residual stresses towards lower stresses was determined. In some investigations the magnitude of the residual stresses decreased with increasing number of cycles whereas in others they stayed stable after the first few cycles.

In most cases an assessment of the stability of welding residual stresses is performed by considering the local elastic–plastic behavior in the notches of the weld. Great efforts have been made by Lawrence and co-workers [8, 20] to determine the local stress–strain behavior by strain-based concepts. Further relaxation of residual stresses was considered by using

J. Baumgartner (✉) · T. Bruder
Fraunhofer Institute for Structural Durability and System
Reliability LBF, Darmstadt, Germany
e-mail: joerg.baumgartner@lbf.fraunhofer.de

material data, which was derived from relaxation tests on smooth specimens. But also quite recently, the elastic–plastic material behavior in the notch was used for assessing the residual stresses in the weld [12, 38].

These investigations contribute to the complex subject in order to get a better understanding on how residual stresses influence the fatigue strength of welded components.

2 Experimental investigations

2.1 Manufacturing

For the analysis of the influence of residual stresses on the fatigue strength of welded components non-load carrying longitudinal stiffeners were chosen. From many investigations it is known that these specimens may exhibit high tensile residual stresses in a distance between 1 and 2 mm from the weld toe [7, 28, 37]. The geometry of the longitudinal stiffeners was adopted from [37] (Fig. 1).

The joints were made from fine-grained steel S460NL (1.8903). This medium-strength steel was chosen, since welding residual stresses were expected to increase with the yield strength. The chemical composition and the quasi-static material properties are given in Tables 1 and 2.

Both, main plate and stiffener were saw cut out of the sheet. The milling direction coincides with the longitudinal direction of the specimens. Before welding the main plate was clean blasted to remove the mill scale. At the edges of the stiffeners a chamfer of 45° was applied to assure a through-welded connection and to avoid root cracks. The stiffeners were positioned by tack-welding on the main plate.

The specimens were robot welded using a gas metal arc welding process. The stiffeners are connected to the base plate by three weld passes, one root pass and two capping passes. For all passes the arc current and the arc voltage were kept constant at I=155 A and U=26 V. The welding speed varied between 15 cm/min to 32 cm/min. All welds were created in the horizontal position (2 F). Filler wire from steel 1.5130 was used, having similar mechanical properties as the base material.

After welding some of the longitudinal stiffeners have been heat treated for 26 h at 580 °C under air atmosphere to reduce residual stresses. To ease the efforts for crack initiation monitoring, the weld toes of three of the four fatigue-critical wrap-around welds were ground using corundum grinders.

2.2 Characterization

For each specimen the angular distortion was measured. It varied between 0° and 2°. To avoid unwanted correlation between distortion and load amplitude applied (i.e., testing only specimen with high distortion at low levels, and vice versa), the specimens were classified and assigned to specific load amplitudes prior to testing.

The weld toe radii were measured using micro-sections and high-resolution contour measurements (Fig. 2). An average radius of around r=50 μm could be identified. The weld opening angles varied between θ=95° and θ=155°. No "weld defects" like cold laps or undercuts were found.

The hardness close to the fatigue-critical weld toe was measured (Fig. 3). The heat-affected zone (HAZ) of the specimens in the as-welded condition showed a hardness peak of over 400 HV1 close to the weld metal (WM) and the weld toe. The base material (BM) has a hardness of 220 HV1, the weld metal of 250 HV1. Due to the stress relieve treatment the hardness is reduced around 15 %.

Welding residual stresses were measured by X-ray diffraction close to the weld toe (Fig. 4). Three independent measurements-series were performed on different specimens, using various measurement equipment (mobile and stationary) and varying collimator sizes. It can be seen, that the residual stresses reach a maximum in a distance of approximately 1.5 mm from the weld toe. Closer to the weld toe the residual stresses decrease, whereas a deviating course can be seen between the measurement of ifs and IWM.

Residual stresses close to zero were measured at the joints in stress relieved condition.

The stability of the residual stresses under cyclic loading was determined by X-ray measurements in LBF in a distance of 1 mm from the weld toe using a collimator diameter of

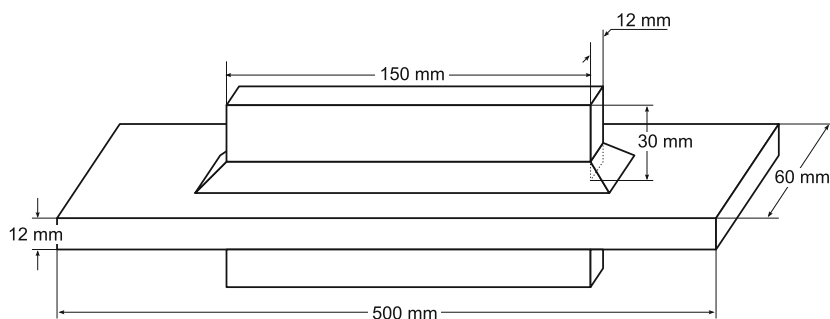**Fig. 1** Geometry of the longitudinal stiffeners

Table 1 Chemical composition (%) of the structural steel 1.8903 according to DIN EN 10 204

C max	Si max	Mn	P max	S max	Al min	Cr max	Mo max	Cu max	Ni max	V max	N max	Nb	Ti
0.20	0.60	1.00–1.70	0.025	0.020	0.020	0.30	0.10	0.55	0.80	0.20	0.025	0.05	0.05

d=2 mm (Fig. 5). All measurements were performed at the specimens located in the test machine, first in unclamped condition, second in clamped condition, and in the following in clamped but unloaded condition after a certain number of cycles. In the unclamped condition the residual stresses equals the welding residual stresses. During the subsequent measurements at the specimens in clamped condition, additional clamping stresses are superimposed.

The evolution of local strains close to the weld toe under cyclic loading was determined on several specimens by strain measurements using strain gauges. Therefore, three strain gauges were applied in short distance from the weld toe in order to measure strains in loading direction (Fig. 6). To measure nominal strains, an additional strain gauge was applied at half of the distance between the clamping and the weld toe.

At some specimens local yielding at strain gauge 1 occurs during clamping (Fig. 7). This can be identified by unclamping the specimen prior to the first loading cycle. After the second clamping the same strain reading as after the first clamping is reached again. Major plastic strains up to ε_x=8.000 µm/m are measured at the first load peak of F_{max}=120 kN. No change in strains can be identified during the subsequent load steps. Such measurements were conducted with similar results at several specimens in the as-welded condition.

Additional information on the residual stresses can be derived from a further evaluation of the strain measurements. When clamping starts, the four strain gauges readings increase proportionally; this indicates linear-elastic behavior. With higher clamping forces the strain at gauge 1 increases disproportionally compared to strain gauge 2. This nonlinearity indicates the start of local yielding.

For specimen P94, Fig. 7, local yield starts at a strain of $\Delta\varepsilon_x$=750 µm. With the simplistic assumption of a uniaxial stress-state and Hooke's Law a stress of $\Delta\sigma_x \approx E \times \Delta\varepsilon_x$=160 MPa at yield is derived. With the yield stress of the base material of σ_Y=450 MPa a residual stress of σ_{RS}=290 MPa can be estimated.
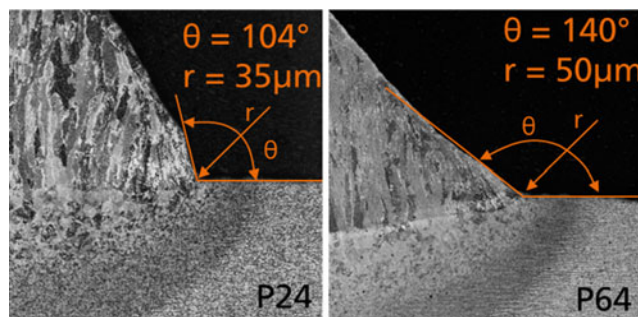
Despites the simplistic assumption, the estimation agrees well with the high residual stresses measured by X-ray method given in Fig. 4.

2.3 Fatigue tests

The fatigue tests on the longitudinal stiffeners were carried out under axial constant amplitude loading in a 250 kN resonance pulsator at frequencies between 32 and 35 Hz. The specimens were clamped over a length of 80 mm at both ends. Overall five test series have been conducted. Four series with specimens in as-welded and stress relieved condition at R=−1 and R=0 as well as a single test series in as-welded condition with R=−1, for which five times a preload of F_{max}=120 kN has been applied.

On all specimens a single strain gauge has been applied at half of the distance between the clamping and the weld toe. The strains after clamping as well as the minimal and maximal strains during the first loading cycles were recorded. From the strain gauge readings R-ratios R<0.75 are derived (Fig. 8). These R ratios result from the angular distortion of the specimens. The stresses induced in the longitudinal direction due to clamping are in the following denoted as "clamping stresses".

Additionally, the crack initiation and propagation was recorded with a digital camera. Recognizability was improved by painting the weld with a mixture of zinc-oxide and glycerin. This painting changes its color from white to black when a crack of technical size (crack depth $a \approx$ 0.1 mm) is initiated. This failure criterion, in the further denoted as "crack initiation" (first change in color of the zinc-oxide) and the criterion of "final rupture" are used. From the experimental results five S-N curves are derived (Figs. 9, 10, and

Table 2 Mechanical properties of the structural steel 1.8903 (S460NL)

Steel	R_m (MPa)	R_{p02} (MPa)	A_5 (%)
1.8903	610	450	17

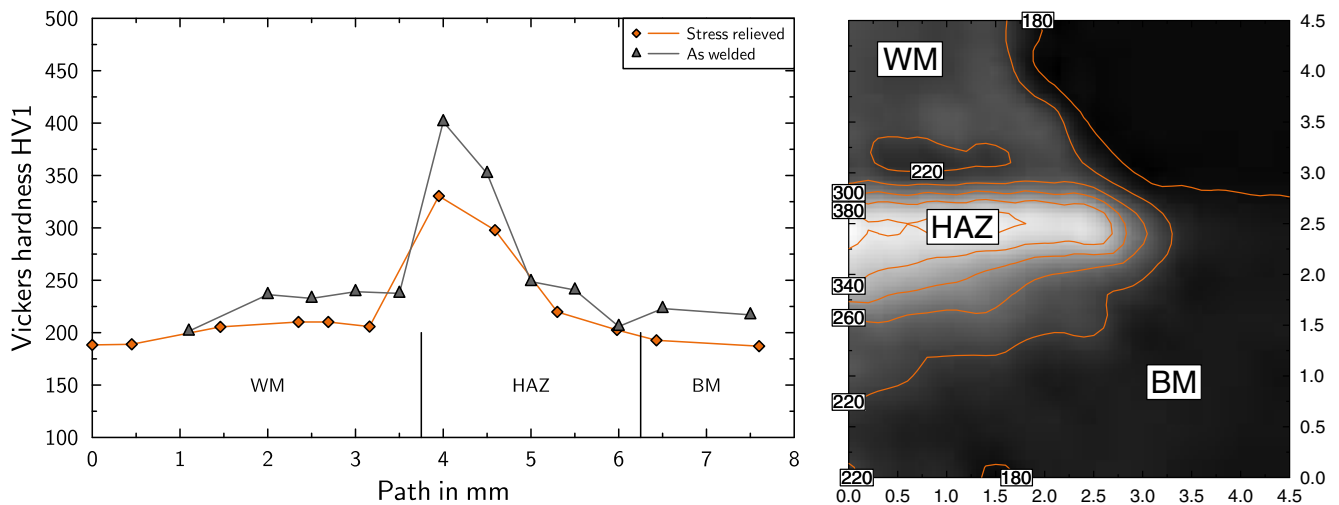**Fig. 2** Local weld geometry and microstructure

Fig. 3 Vickers hardness HV1 (*left*) and local micro-hardness HV01 (*right*) for a specimen in as-welded condition

11). Nominal stresses are calculated in the net section, neglecting the stiffeners. The results of the fatigue tests are summarized in Table 3.

Whereas the fatigue strength of the specimens in as-welded condition is independent of the load ratio, Fig. 9, a mean stress sensitivity of $M=0.33$ at $N=10^7$ cycles is identified for the specimens in stress relieved condition (Fig. 10). In the tests with $R=-1$, a slight change in slope is observed from $k=3$ for the as-welded condition to $k=3.5$ for the stress relieved condition.

The scatter of the tests on joints in as-welded condition is (in accordance with literature data [15]) remarkably low,

having a scatter of $1:T_\sigma=F_a(P_S=10\ \%)/F_a(P_S=90\ \%)=1.23$. With stress relieve treatment an increase in scatter to $1:T_\sigma>1.40$ is observed. This behavior can be explained by the individual distortion of the specimens. Since the distortion is nearly proportional to (mostly tensile) clamping stresses, in more distorted specimens higher clamping stresses are induced, leading to a decrease in fatigue life. Vice versa, for less distorted specimens a longer fatigue life is expected.

The load ratio measured with strain gauges for clamping and loading, Fig. 8, helps to understand this effect. Using the measured R ratios the results of each individual fatigue test on stress relieved specimens is converted to $R=-1$ using mean stress sensitivity factors M (Fig. 12). This approach allows subsuming all fatigue data into a single S-N curve with a low scatter. A minimum scatter of $1:T_\sigma=1.38$ is achieved with $M(-1\leq R\leq0)=0.07$ and $M(R>0)=0.17$.

Compared to the specimens in as-welded condition the overload of 5×120 kN leads to an increase in fatigue strength (Fig. 11). This increase is primarily caused by an increase of the cycles to crack initiation. The ratio between cycles to crack-initiation N_i and cycles to final rupture N_r is reduced to $N_i:N_r\approx1:3$ in the test with overload compared to a ratio of $N_i:N_r<1:10$ for specimens tested with constant amplitude loading.

The test results of all joints in as-welded condition and joints in stress relieved condition with R ratio $R=0$ can be comprised in a single S-N curve for crack propagation (Fig. 13). Only the specimens in stress relieved condition with $R=-1$ show a longer crack propagation phase, which might result from the lower tensile mean stresses. These test results were excluded from calculation of the scatter.

Looking closely at the S-N data, Figs. 9, 10, and 11, some specimens can be identified with a relatively long fatigue life
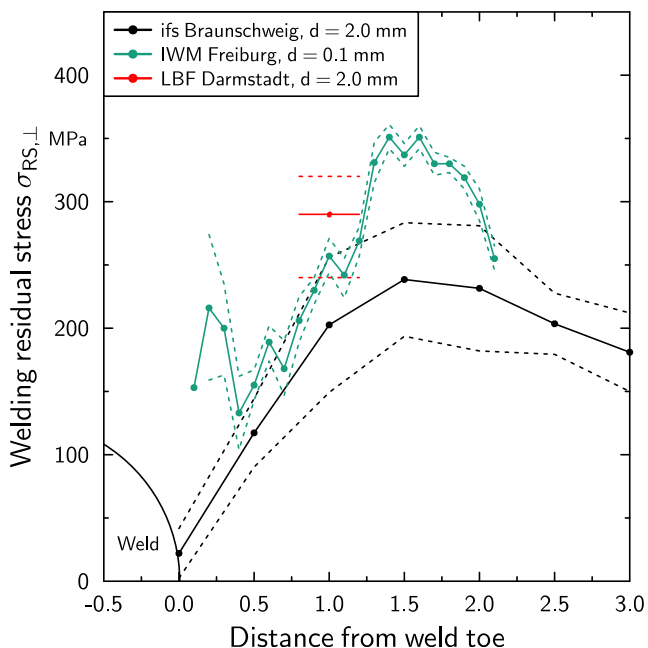

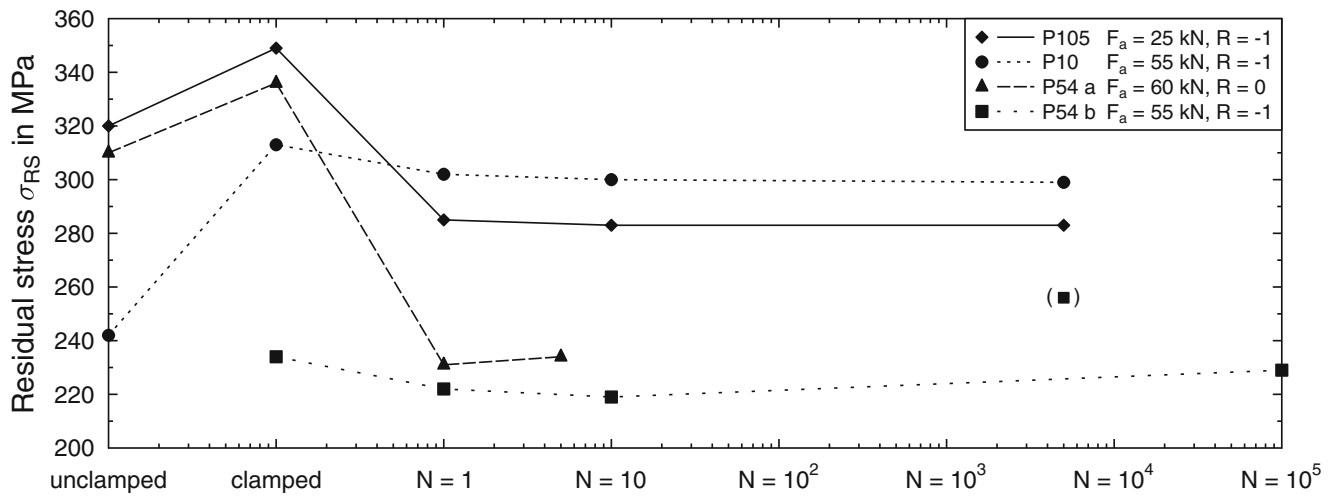Fig. 4 Measured welding residual stresses perpendicular to the weld

Fig. 5 Residual stress relaxation during fatigue testing for various specimens

compared to the majority of the specimens. These specimens had a comparatively smooth weld profile (low flank angle and large notch radius) and have been excluded before calculating the scatter band.

3 Numerical analysis

3.1 Finite element model

For further analyses, finite element models of the longitudinal stiffeners were set up. For the global geometry tetrahedron elements with quadratic shape function were used. The fatigue

critical weld area was meshed using hexahedron elements with quadratic shape function and created using the sweep function. The local element length at the weld toe was chosen in accordance to the stress gradient in order to receive converged notch stresses [3]. Both parts were tied together using ABAQUS "TIE" function. The local weld geometry was partitioned to map roughly the local hardness distribution (Fig. 14).

3.2 Stress concentration factors

Stress concentration factors K_t were calculated for various notch radii and weld angles using linear elastic material behavior (E=210 GPa, ν=0.3; Table 4).

Fig. 6 Location of strain gauges for measuring the local strain evolution during clamping and loading
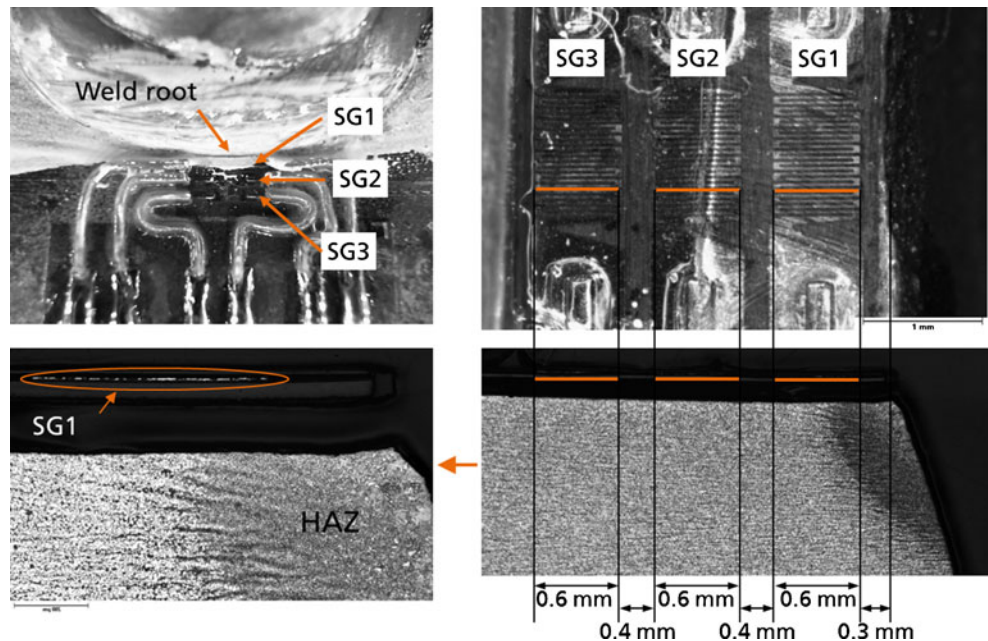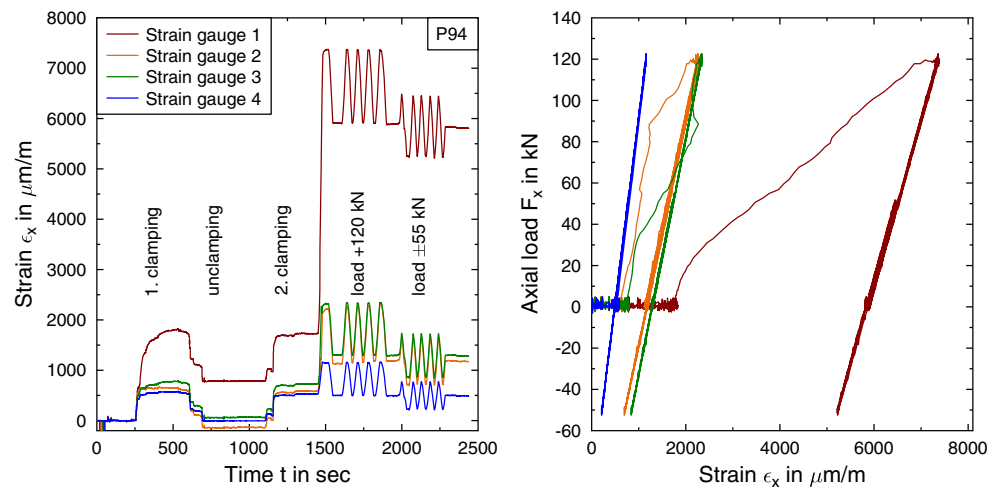
Fig. 7 Strains measured during clamping and loading

3.3 Elastic–plastic stress–strain behavior

For the elastic–plastic FE calculations the stabilized cyclic stress–strain curve was estimated with the Uniform Material Law (UML) [2] based on the simplified hardness distribution as shown in Fig. 14. Since there is no material model in ABAQUS which considers a "simplified" material behavior (kinematic hardening as well as the Masing's Assumption and the memory effect) as it is often used in strain-based approaches, the combined isotropic/kinematic hardening model in ABAQUS (Frederick-Armstrong type) has been applied, which additionally covers ratcheting effects. This model uses the von Mises yield criterion. The model parameters (yield stress and two back-stress tensors) were adjusted to fit the stabilized stress–strain curve derived from UML (Table 5). Furthermore, the Seeger-Beste approximation formula [34], was applied.
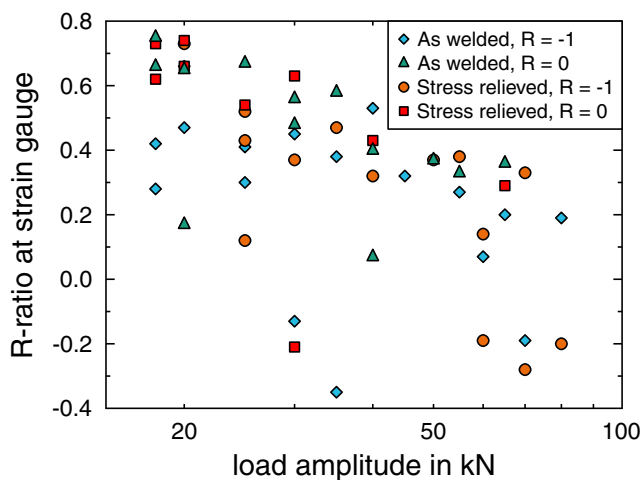

Fig. 8 R-values from strain gauge readings for each specimen depending on clamping and external loading

The cyclic stress–strain curve of the weld material was described with the Ramberg-Osgood equation [33] and its constants K'=1,252 MPa and n'=0.15.

The elastic–plastic behavior was calculated for two models of the longitudinal stiffener with a notch radius r=0.05 mm and a weld angle α=90° as shown in Fig. 14 (left). In one model the "realistic" hardness distribution as shown in Fig. 14 was used, in the other "simplified" model the material properties of the weld metal were assigned for all partitions. A comparison between the calculated stresses and strains for initial loading shows only minor differences for both FE-models (Fig. 15). The Seeger-Beste formula fits quite well with the solution derived by finite element analysis. A slight overestimation of the strain can be identified.

Having proved the applicability of the Seeger-Beste formula, a simplified calculation of the local stress–strain behavior was carried out. Following approach was used:

- Since the exact weld geometry (at the location of crack initiation for each individual specimen) could not be measured, an average geometry (r=0.05 mm and α=60°) was assumed for the calculation.
- The measured welding residual stresses of σ_{RS}=250 MPa, determined as average value in an area of 2 mm from the weld toe, Fig. 4, were applied, conservatively, like nominal mean stresses for the specimens in as-welded condition.
- For each specimen nominal mean stresses were applied to simulate clamping, using the individual strain gauge reading obtained during the fatigue tests.
- The local stress–strain hysteresis loop was calculated for a single load cycle using the Seeger-Beste formula.
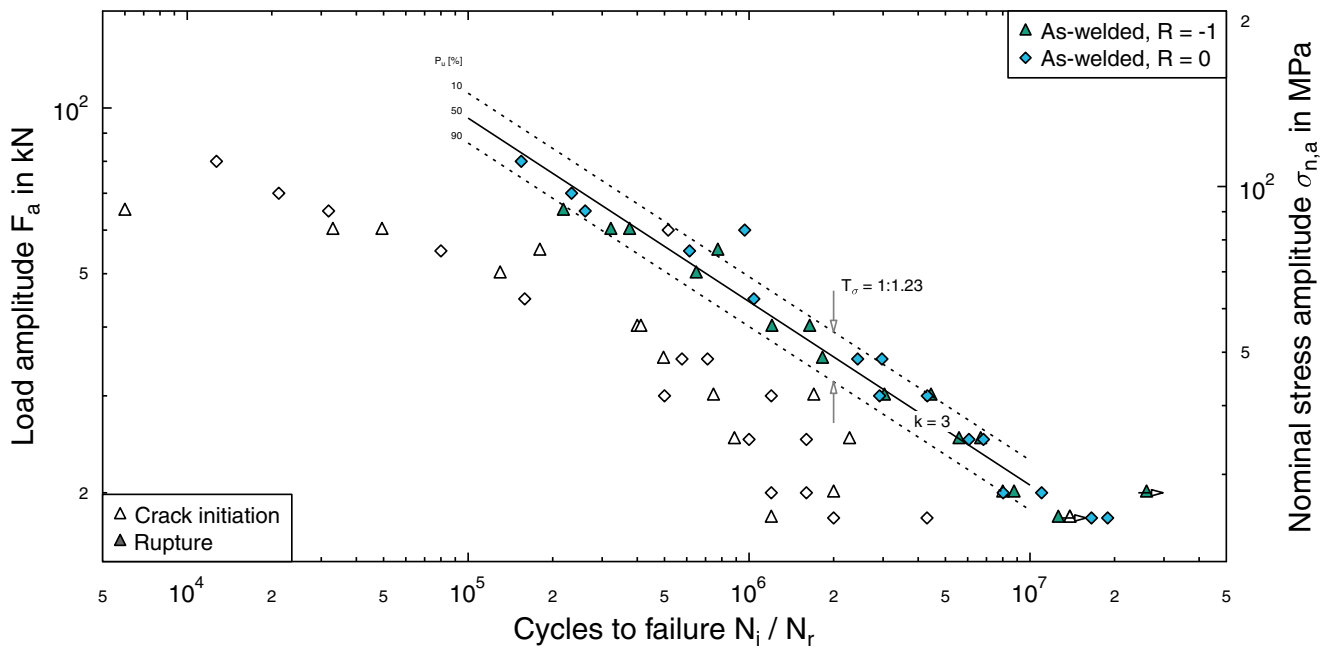- Conservatively, no further cyclic mean stress relaxation was assumed.

Fig. 9 Fatigue tests, specimen in as-welded condition

Following the approach described above, stress–strain hysteresis loops are derived for each individual test. Due to the high mean stresses (resulting from residual stresses and clamping) as well as the high stress concentration factor at the weld toe, the local mean stresses are reduced at the weld toe. This effect is more pronounced for the specimens with high angular distortion tested at high load levels.

3.4 Fatigue assessment

An assessment of the local stress–strain hysteresis loops was performed using the Smith-Watson-Topper damage parameter P_{SWT} [36].

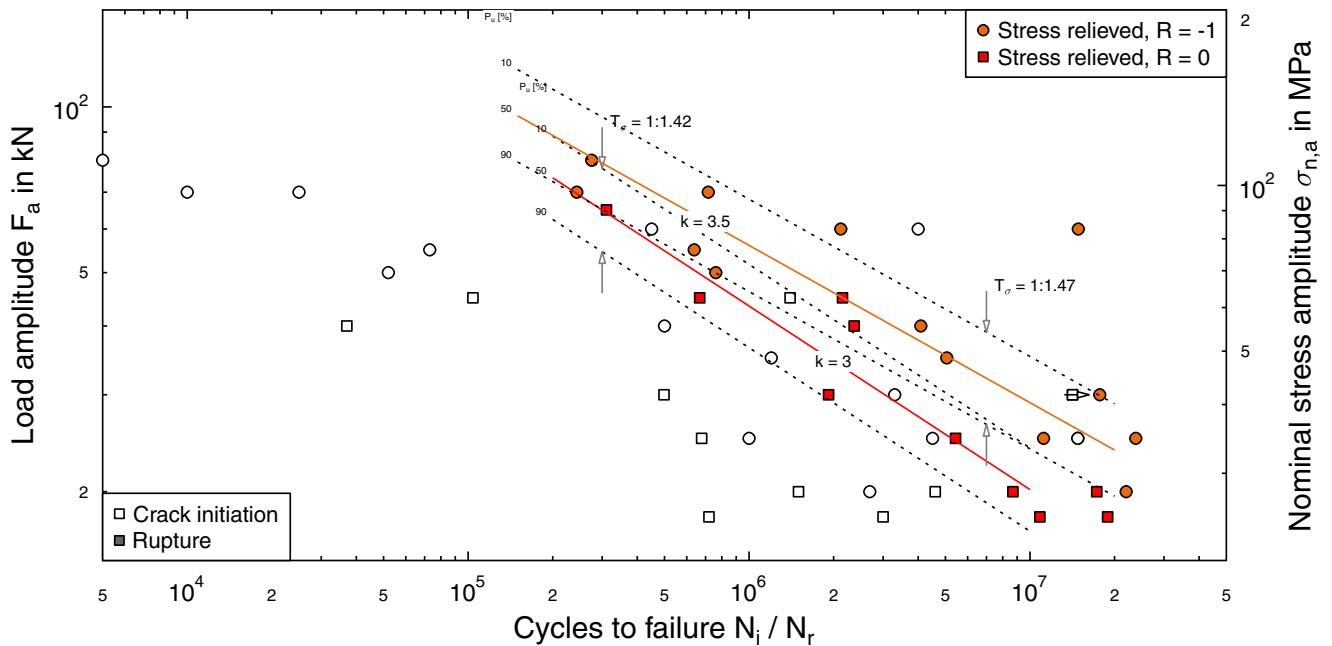$$P_{SWT} = \sqrt{\varepsilon_a(\sigma_a + \sigma_m)E}$$

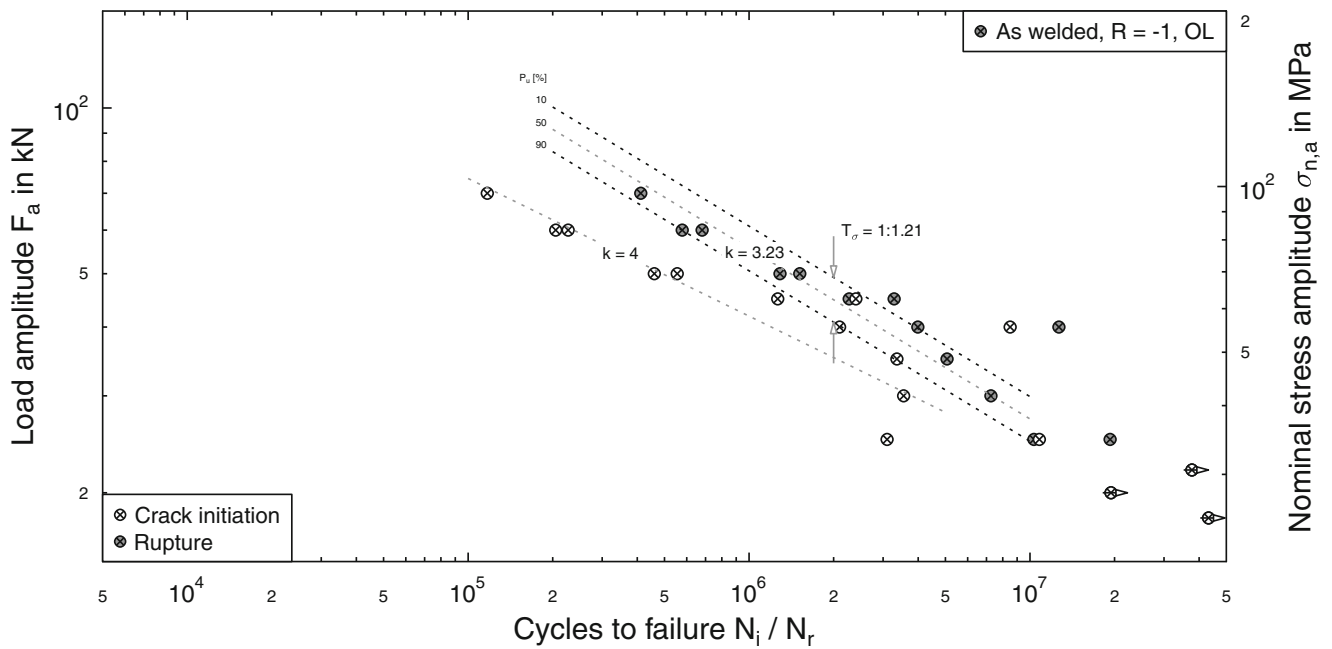**Fig. 10** Fatigue tests, specimens in stress relieved condition

Fig. 11 Fatigue tests, specimens in as-welded condition after initial overloads with $F_{max}=120$ kN

Since this damage parameter is overestimating the influence of mean stresses for $\sigma_m<0$ ($\sigma_m\leq-\sigma_a$ yields to $P_{SWT}=0$ neglecting any damaging effects), a minimum R value of $R=-1$ is assumed for all cycles with $\sigma_m<0$. For all fatigue data, the endurable nominal stresses were transformed to P_{SWT} values (Fig. 16). Following this approach a P_{SWT}-N curve can be derived having a remarkable low scatter of $1:T_P=1.20$ for the failure criterion of "rupture".

The specimens marked by brackets had a significant longer life. These specimens have a particularly low weld angle and were therefore excluded from the calculation of the scatter band.

The specimens with overloads prior to testing fit quite well in the scatter band. Only for lower load amplitudes the positive effect of the overload on the fatigue strength is overestimated.

Typically, the local strain approach is applied only for the failure criterion of "crack initiation". Figure 16 shows that the applied approach also reduces the scatter for the failure

criterion of "crack initiation". A generally higher scatter for crack initiation compared to rupture is well-known from literature. The P_{SWT}-N curve derived for the weld metal from the Uniform Material law lies by a factor of 1.5 beneath the P_{SWT}-N curve for the joints and its failure criterion of crack initiation.

The deviation between both P_{SWT}-N curves may be linked to size effects, which are not covered by the damage parameter P_{SWT} and have to be considered additionally. These size effects may be based either on further support effects (micro-support) or on statistical effects.

The stress averaging approach according to Neuber [31] is one of many methods to account for the influence of stress gradients on the fatigue strength. This approach uses the stress course in the notch ligament derived from an elastic stress analysis to determine a support factor n

$$\frac{1}{n} = \frac{1}{\sigma_{max}} \frac{1}{\rho^*} \int_0^{\rho^*} \sigma(x)dx$$

Table 3 Fatigue test results, overview

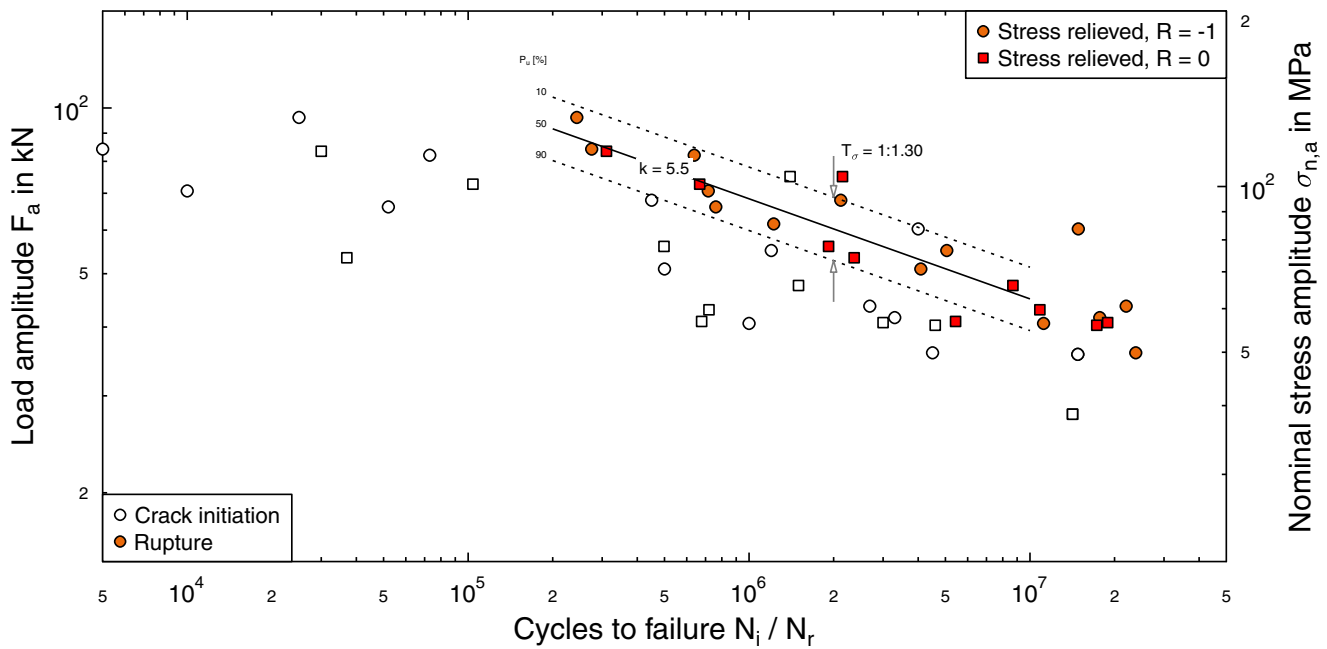| Test series	$\sigma_{n,a}$ ($N=2\times10^6$, $P_S=50$ %) in MPa	k	$1:T_S$	M ($N=2\times10^6$)
As-welded, $R=-1$	49.9	3.1	1.15	0.02
As-welded, $R=0$	49.0	3.0	1.23	
Stress relieved, $R=-1$	63.8	3.5	1.47	0.33
Stress relieved, $R=0$	47.9	3.0	1.42	
As-welded, $R=-1$, OL	62.6	3.2	1.21	–

Fig. 12 Fatigue test results for specimens in stress relieved condition converted to $R=-1$ as described in the text

Principally, all methods using stress gradients from elastic analyses to derive support factors are defined only at load levels, which lead to an elastic local response. Therefore, support factors n_e have to be derived from fatigue data in the very high cycles fatigue regime [35]. For the calculation of the support factor for the assessment of the longitudinal stiffeners, a micro-support length of $\rho^*=0.09$ mm was used for the failure criterion "crack initiation" [4].

The damage parameter P_{SWT} of the stiffeners is modified to

$$P_{SWT^*} = \frac{1}{n_e} \cdot P_{SWT}$$

Using this approach, P_{SWT^*} values can be derived for each single fatigue test (Fig. 17). Comparing the P_{SWT} values for the stiffeners and those for the weld metal derived by the
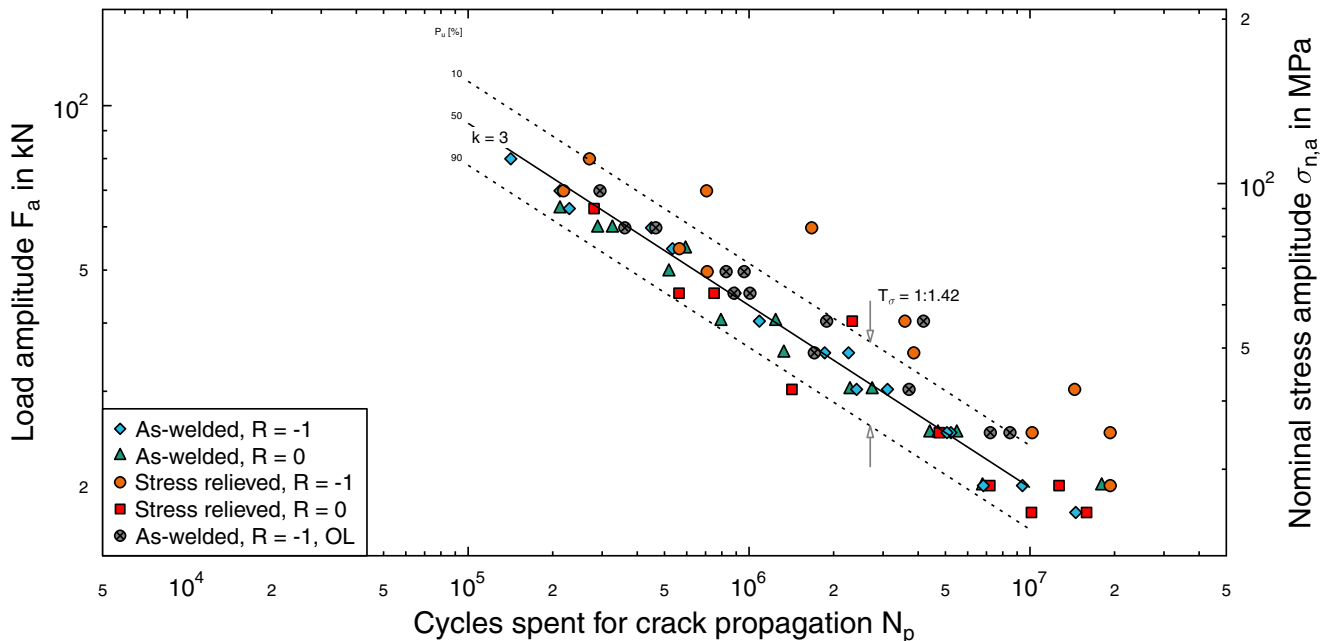

Fig. 13 Crack propagation S-N curve for all specimens, regression of the S-N curve excluding the joints in stress relieved condition with $R=-1$
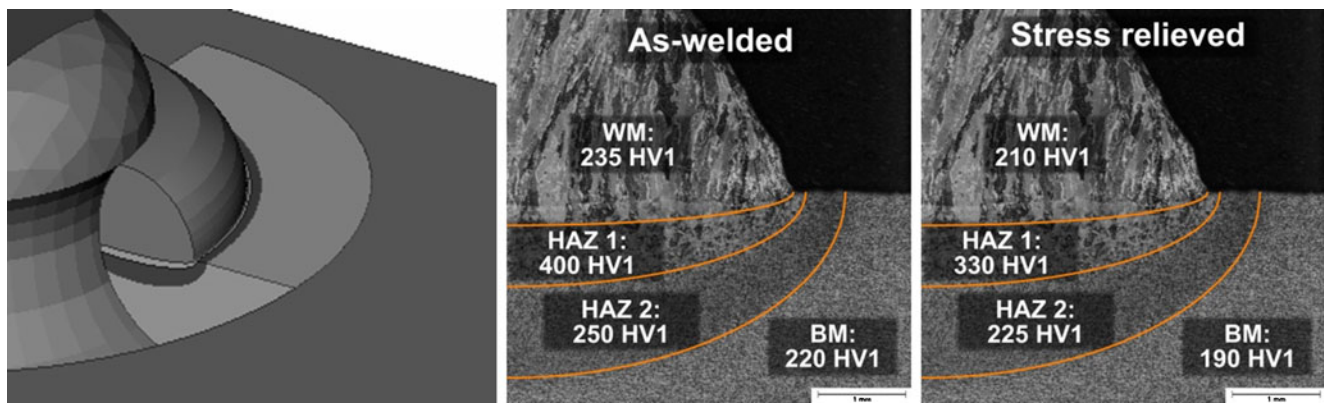
Fig. 14 Modeling of the weld in the FE model (*left*) using partitions related to areas with uniform microstructural hardness (*right*)

Uniform Material Law [2] a significant difference can be seen. This difference results from an overestimation of the support effects calculated at the stiffeners.

4 Discussion

4.1 Fatigue strength of longitudinal stiffeners

At first, the derived fatigue data [1, 5, 7, 9–11, 14–18, 20, 23, 24, 26–28, 30, 31, 33, 38, 41] are compared with data from literature and the class FAT71 (stiffener length up to $l_s \leq 150$ mm) proposed by the IIW recommendations (Fig. 18). More than 600 fatigue tests are taken into account. Generally, the class FAT71 as recommended by the IIW recommendations is able to subsume the test data conservatively. For the joints in stress relieved condition, a slightly higher fatigue strength might be assigned. Further statistical analyses were not performed due to the high scatter and the variation in the number of cycles n_{ro} used to determine run-outs, $10^6 < n_{ro} < 10^8$.

In Fig. 18, the region with less than $N = 1 \times 10^6$ cycles the fatigue data can be covered with a scatter of $1:T_\sigma = 1.50$ for the specimens in as-welded condition, despite the heterogeneous data base. A significant influence of the R ratio, the material strength, or the geometry cannot be identified. In the high cycle fatigue region the scatter increases.

It is likely that this effect is caused by local mean stresses as well as residual stresses close to the weld toe. On high load levels major local yielding occurs in the sharp toe notches equalizing the level of local mean stresses in between various joints. At lower load levels the local notch stresses might not exceed the local yield stress and therefore the level of local mean stresses, which vary from joint to joint, may lead to an additional source of scatter in fatigue life. This hypothesis may be verified by local elastic–plastic calculations based on local material, geometry, and loading data. Unfortunately, for most fatigue tests on longitudinal stiffeners reported, important influence factors (like distortion, clamping conditions, local weld geometry as well as the local hardness at the weld notches) on the fatigue strength were not given in detail. Therefore, a thorough re-evaluation of significant amount of fatigue data is hindered to a great extent.

4.2 Influence of main geometric dimensions

To analyze the influence of the geometry parameters of longitudinal stiffeners on fatigue strength, endurable nominal stresses for the various test series shown in Fig. 18 are computed. These stresses are plotted versus geometrical parameters, the main plate width, the attachment length as well as the ratio between the main plate width and the sheet thickness B/t (Fig. 19). Additionally, parametric FE models were set up with a constant thickness of the main and the attachment plate ($t = 12$ mm), whereas the plate width and the

Table 4 Stress concentration factors K_t for various notch radii and weld angles using maximum principal stresses

$r \backslash \alpha$	30°	45°	60°	75°	90°
0.05 mm	5.49	8.04	10.34	12.05	13.14
0.20 mm	3.93	5.14	6.12	6.75	6.97
1.00 mm	2.64	3.08	3.37	3.56	3.65

Table 5 Material parameters for the Ramberg-Osgood equation (K' and n') and for the ABAQUS material model (yield stress σ_0 and back-stresses: C_1, γ_1, C_2, γ_2)

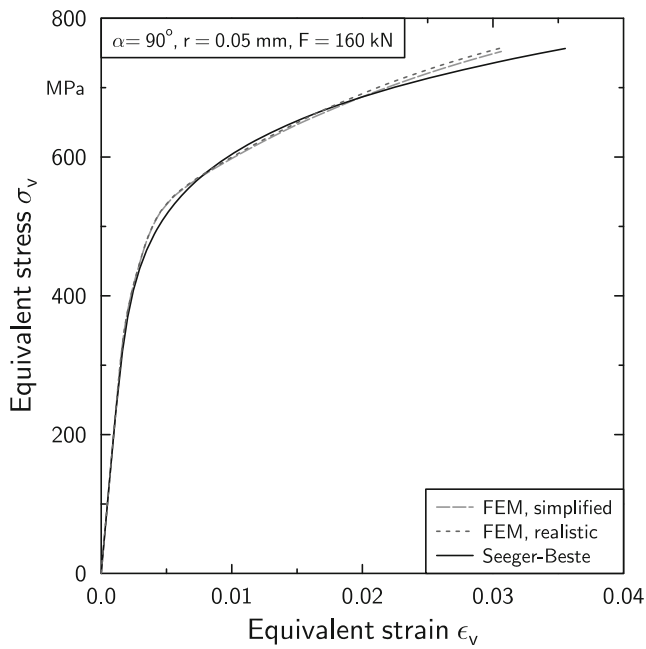| Area	HV1	R_m	K'	n'	σ_0	C_1	γ_1	C_2	γ_2
BM	220	711	1,172	0.15	260	150,000	1,050	13,000	48
HAZ 2	250	808	1,332	0.15	350	200,000	1,100	16,000	42
HAZ 1	400	1,292	2,132	0.15	550	300,000	950	24,000	40
WM	235	759	1,252	0.15	320	200,000	1,100	16,000	46

Fig. 15 Local stress–strain behavior in the weld toe notch derived by finite element analysis and the Seeger-Beste approximation for the initial loading

stiffener length were varied. Varying the stiffener length, the distance between clamping and stiffener was kept constant. For a weld opening angle of $\theta=120°$ and a weld toe radius of $r=1.0$ mm stress concentration factors K_t were calculated. For the longitudinal stiffeners tested within this investigation endurable notch stress ranges at

$N=2\times10^6$ cycles ($\Delta\sigma_e=330$ MPa for $\theta=120°$ and $P_s=50$ %) are derived. Dividing these notch stresses by K_t results in nominal stress ranges $\Delta\sigma_{n,2E6}$ for $P_s=50$ % depicted by the curves in Fig. 19.

These curves (FEM, $t=12$ mm) show that the stress concentration factor K_t depends strongly on the main plate width B as well as the ratio between the main plate width and the sheet thickness B/t. In the range of 50 mm$\leq B\leq$320 mm the stress concentration factor K_t increases by 30 %. An increase of the stiffener length l_s in the range from 50 mm$\leq l_s\leq$250-mm leads to an increase of K_t by less than 3 %. In contrast to this results stand the FAT classes from the IIW recommendations, in which the stiffener length is the main influencing factor on the fatigue strength of longitudinal stiffeners. For a further judgment a thorough analysis of the background and experiments leading to the current recommendation is suggested.

Whereas the individual results incorporate the influence of various parameters, for the calculated curves only a single parameter was varied. Nevertheless, for the main parameters B and B/t individual results and plotted curves describe a similar tendency considering the fatigue data of the as-welded specimens.

4.3 Local elastic–plastic approach

Local elastic–plastic approaches are able to describe the material behavior under cyclic loading. Dependent on the complexity of the approach chosen, phenomena like residual
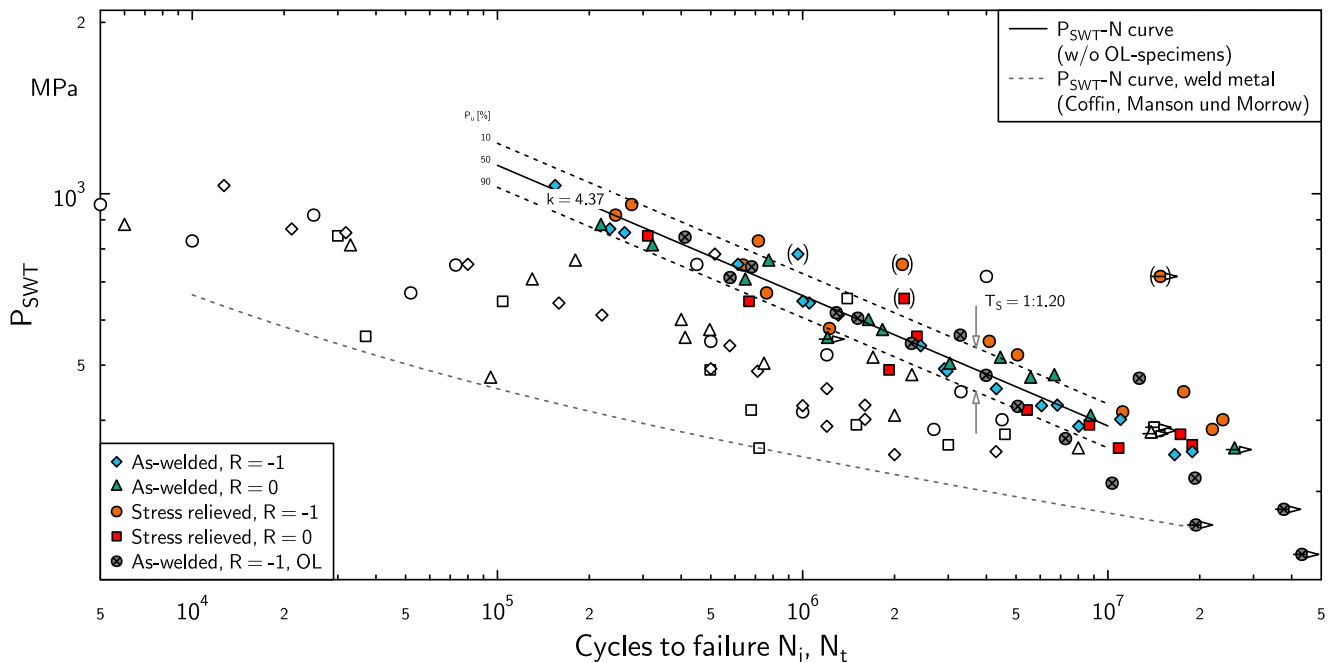

Fig. 16 P_{SWT}-N curve derived from all fatigue tests using a weld toe radius of $r=0.05$ mm
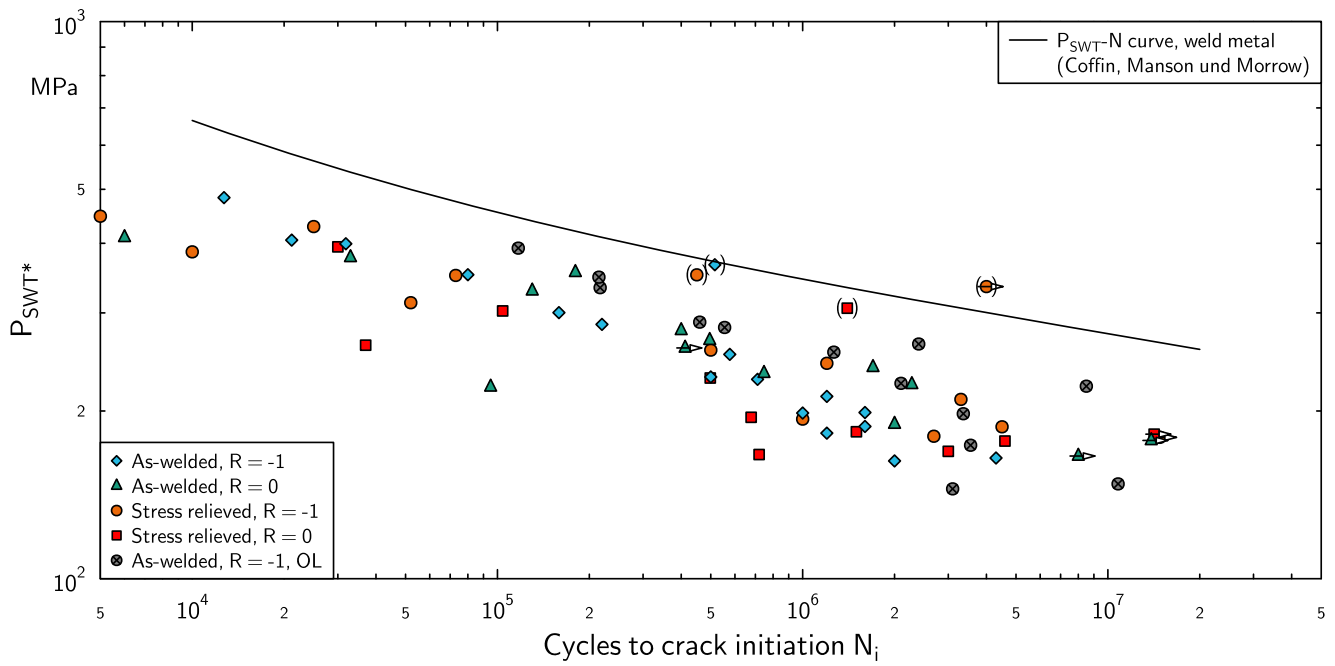
Fig. 17 P_{SWT*}-N curve derived from all fatigue tests using a weld toe radius of $r=0.05$ mm and regarding size effects in comparison with the P_{SWT}-N curve of the weld metal

stress relaxation can be calculated on a cycle-by-cycle basis. As mandatory requirements for the application two aspects have to be satisfied. Firstly, validated material models describing local

effects have to be available. Secondly, necessary material data have to be known, which are subject of high gradients (i.e., hardness) in welded joints. Additionally, inner variables like
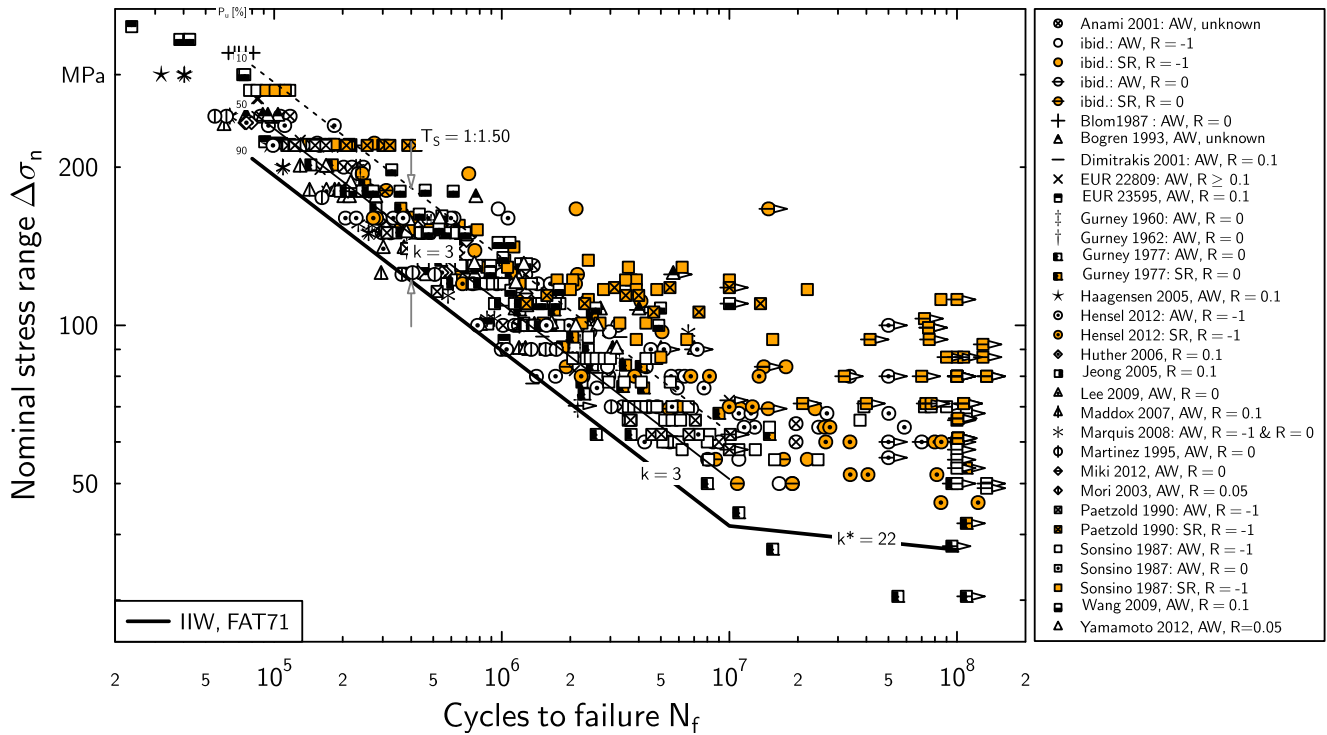

Fig. 18 Comparison between fatigue tests on longitudinal stiffeners and S-N curve for FAT71. Joints in stress relieved condition are designated by orange color
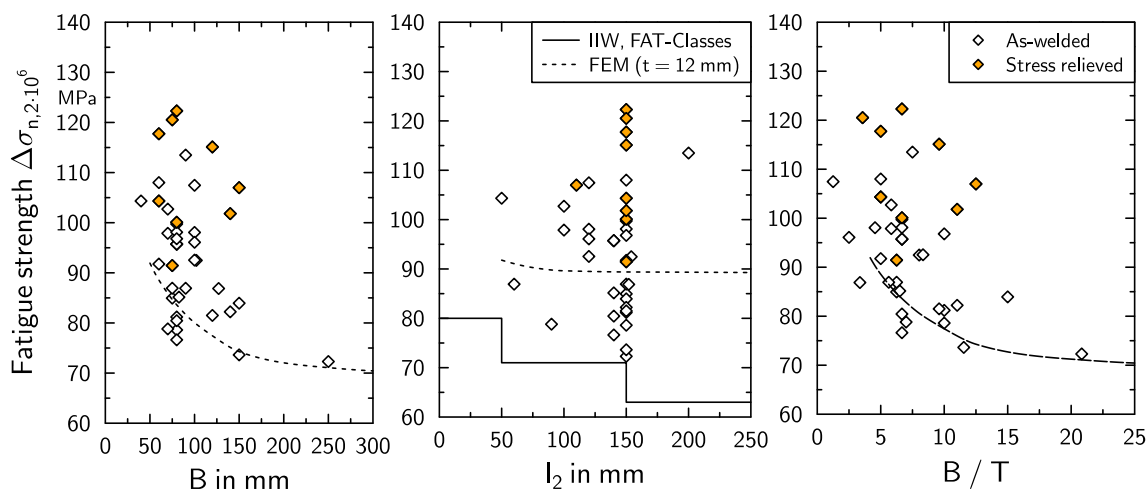
Fig. 19 Correlation between geometrical dimensions and fatigue strength

hardening or back stresses are set during the welding process and therefore non-zero before the loading starts.

It is obvious that a fatigue assessment which takes care of all these aspects is not feasible economically and even highly demanding in a technical way. Therefore, a simplified approach was chosen which neglects some effects and covers others in a conservative manner. An easy applicability is assured, since only the load–strain relation needs to be calculated. This can be performed by simple formulae. The main parameters regarded are summarized in the following.

The choice of the geometry used in calculation models is important, since the local geometry has a high influence on the stress concentration and, in combination with the external loading, on the magnitude of local stresses. Therefore, average toe radii and weld angles have been used. Since the fatigue crack initiates at the weld toe, the cyclic material data of the weld material given by the Uniform Material Law was used.

The experimental results obtained at the longitudinal stiffeners as well as the fatigue data taken from literature suggest that the local mean and residual stresses play a major role in the fatigue life. Simplifying, clamping and residual stresses were applied like external loads. Mean stress relaxation and ratcheting were not considered, because they were not observed in the fatigue tests. The impact of the local stress–strain hysteresis loops on fatigue is taken into account by the damage parameter P_{SWT}.

Further effects that have not been considered are: multiaxial stress states, cyclic hardening or softening of the material as well as other material variables. In addition further non-local effects have been ignored.

As shown in Fig. 16, this approach allows to subsume the test results of the longitudinal stiffeners in a damage parameter–life curve (P_{SWT}-N) with a small scatter band. By comparison of both P_{SWT}-N curves, for the joints and for the base

material, a higher deviation could be identified which was attributed to support effects. By using the stress averaging approach according to Neuber and considering only elastic stresses, the support effects were overestimated. So it is still unknown what kind of effect (micro-structural support, statistical size effect…) predominates and have to be included in a strain-life assessment of welded components. But it seems obvious that the effect is connected to the stress gradient in the notch ligament.

5 Conclusions

In this investigation fatigue tests under constant amplitude loading have been performed on longitudinal stiffeners in order to understand the influence of residual stresses on the fatigue strength. Following main conclusions can be drawn:

- The angular distortion of the specimens leads to high local stresses after clamping which influence the fatigue strength especially at low amplitudes.
- After clamping and the first loading cycle, no major change in residual stresses was measured by X-ray diffraction. Since the residual stresses were measured in a distance of 1 mm from the weld toe (with a diameter of the measurement spot of $d=2$ mm), information on the residual stresses directly at the weld toe with its average radius of $r=0.05$ mm could not be obtained.
- The derived S-N data for the failure criterion of rupture agrees well with data from literature, especially for less than $N=1\cdot10^6$ cycles. The overall small scatter observed at higher load levels ($N<10^6$) may be contributed to mean as well as residual stresses.
- If the average geometry of the weld as well as residual stresses are taken into account, the test results can be

described by a single P_{SWT}-N curve with scatter of $T_P = 1{:}1.20$.

- The deviation between the calculated P_{SWT}-N curve for the weld metal and the joints can be attributed to size effects.
- An initial tensile overload lead to an increase in number of cycles for crack initiation, whereas the number of cycles for crack propagation was nearly equal to other specimens tested at the same load level.

References

1. Anami K, Miki C (2001) Fatigue strength of welded joints made of high-strength steels. Prog Struct Mater Eng 3:84–94
2. Bäumel A Jr, Seeger T (1990) Materials data for cyclic loading, Supplement 1. Elsevier, Amsterdam
3. Baumgartner J, Bruder T (2013) An efficient meshing approach for the calculation of notch stresses. Weld World 57: 137–145
4. Baumgartner J (2013) Schwingfestigkeit von Schweißverbindungen unter Berücksichtigung von Schweißeigenspannungen und Größeneinflüssen (Fatigue strength of welded joints under consideration of residual stresses and size effects), PhD thesis, Technical University of Darmstadt
5. Blom A (1987) Fatigue strength of welded joints subjected to spectrum loading. The Aeronautical Research Institute, Bromma
6. Blom A (1995) Spectrum fatigue behaviour of welded joints. Int J Fatigue 17:485–491
7. Bogren J, Martinez LL (1993) Spectrum fatigue testing and residual stress measurements on non-load carrying fillet welded test specimens, in Proceedings: Fatigue under spectrum loading and in corrosive environments, Technical University of Denmark
8. Burk J, Lawrence F (1978) The effect of residual stresses on weld fatigue life, FCP Report No. 29, University of Illinois
9. Dimitrakis S, Lawrence F (2001) Improving the fatigue performance of fillet weld terminations. Fatigue Fract Eng Mater Struct 24:429–438
10. Maddox S, Hopkin G, Holy A, Branco CM, Infante V, Baptista R, Schuberth S, Sonsino C, Küppers M, Marquis G, Lihavainen V-M, Gales A, denHerder A, Lont M (2007) Improving the fatigue performance of welded stainless steels, EUR 22809 EN, European Commission
11. Zilli G, Maiorana E, Peultier J, Fancia A, Hechler O, Raunert T, Maquoi R (2008) Application of duplex stainless steel for welded bridge construction in an aggressive environment, European Commission
12. Farajian M, Nitschke-Pagel T, Dilger K (2010) Mechanism of residual stress relaxation and redistribution in welded high strength steel specimens under mechanical loading. Weld World 54:366–375
13. Gurney T (1960) Influence of residual stress on fatigue strength of plates with fillet welded attachments. Br Weld J 7:415–431
14. Gurney T (1962) Further fatigue tests on mild steel specimen with artificially induced residual stresses. Br Weld J 8:609–613
15. Gurney T (1977) Residual stresses in welded constructions and their effect, The Welding Institute
16. Haagensen PJ, Alnes O (2005) Progress Report on IIW WG2 Round Robin Fatigue Testing Program on 700 MPa and 350 MPa YS Steels, International Institute of Welding, XIII-2081-05
17. Hensel J, Nitschke-Pagel T, Schönborn S, Dilger K (2012) Factors affecting the knee point position of S-N curves of welds with longitudinal stiffeners, International Institute of Welding, XIII-2441-12
18. Huther I, Pollet F, Lieurade H (2002) Effect of the restraining conditions during welding on fatigue strength, International Institute of Welding XIII-1952-02
19. Huther I, Suchier Y, Lieurade H (2006) Fatigue behaviour of longitudinal non-load-carrying joints improved by burr grinding, TIG dressing, International Institute of Welding, XIII-2108-06
20. Higahsida Y, Burk J, Lawrence FV (1978) Strain-controlled fatigue behavior of ASTM A36 and A514 grade F steels and 5083-O aluminum weld materials. Weld J 57:334–344
21. James M, Hughes D, Hattingh D, Mills G, Webster P (2009) Residual stress and strain in MIG butt welds in 5083-H321 aluminium: As-welded and fatigue cycled. Int J Fatigue 31:28–40
22. Jeong WH, Seung HH, Byung CS, Jae HK (2005) Fatigue crack initiation and propagation life of welded joints. Key Eng Mater 297–300:781–787
23. Lee C-H, Chang K-H, Jang G-C, Lee C-Y (2009) Effect of weld geometry on the fatigue life of non-load-carrying fillet welded cruciform joints. Eng Fail Anal 16:849–855
24. Maddox S (1982) Influence of tensile residual stresses on the fatigue behavior of welded joints in steel, ASTM STP 776. Am Soc Test Mater 63–96
25. Maddox S (2007) Improving the fatigue strength of toe ground welds at the ends of longitudinal attachments, International Institute of Welding, XIII-2156-07
26. Marquis G, Björk T (2008) Variable amplitude fatigue strength of improved HSS welds, International Institute of Welding, XIII-2224-08
27. Martinez LL, Blom AF (1995) Influence of life improvement techniques on different steel grades under fatigue loading. Fatigue Des III
28. Martinez LL, Lin R, Wang D, Blom AF (1997) Investigation of residual stresses in as-welded and TIG-dressed specimens subjected to static/spectrum loading, Proceedings of the North European Engineering and Science Conference, (NESCO): "Welded High-Strength Steel Structures"
29. Miki C, Tai M (2012) Fatigue strength improvement of out-of-plane welded joints of steel girder under variable amplitude loading, International Institute of Welding, XIII-2445-12
30. Mori T, Inomata T (2003) Influence of grinding method on fatigue strength of out-of-plane gusset welded joints, International Institute of Welding, XIII-1970-03
31. Neuber H (1968) Über die Berücksichtigung der Spannungskonzentration bei Festigkeitsberechnungen. Konstruktion 20:245–251
32. Paetzold H, Petershagen H (1990) The effect of post-weld explosion treatment on the fatigue strength of plates with longitudinal stiffeners, International Institute of Welding, XIII-1369-90

33. Ramberg W, Osgood WR (1943) Description of stress–strain curves by three parameters, NACA technical notes, No. 902, National Advisory Committee for Aeronautics

34. Seeger T, Beste A (1977) Zur Weiterentwicklung von Näherungsformeln für die Berechnung von Kerbbeanspruchungen im elastisch-plastischen Bereich (Improvement of approximation formulae for calculating notch stresses and strains in the elastic–plastic range), in: Fortschrittsbericht der VDI Zeitschriften: Kerben und Bruch (Notches and fracture), Reihe 18, Nr. 2, VDI-Verlag

35. T Seeger (1996) Stahlbau Handbuch 1 Teil B. Stahlbau-Verlagsgesellschaft mbH Köln

36. Smith K, Watson P, Topper T (1970) A stress–strain functions for the fatigue on materials. J Mater 5:767–778

37. Sonsino CM, Böhme D, Kulka C, Helwig R (1987) Slope of the S-N curve and high-cycle fatigue behaviour of longitudinal stiffeners in as-welded and stress relieved states, International Institute of Welding, XIII-1242-87

38. Sonsino C, Kaufmann H, Wagener R, Fischer C, Eufinger J (2011) Interpretation of overload effects under spectrum loading of welded high-strength steel joints. Weld World 55:66–78

39. Trufyakov V (1958) Welded joints and residual stresses. Br Weld J 5:491–498

40. Wang T, Wang D, Huo L, Zhang Y (2009) Discussion on fatigue design of welded joints enhanced by ultrasonic peening treatment (UPT). Int J Fatigue 31:644–650

41. Yamamoto N, Mouri M, Okada T, Mori T (2012) Analytical and experimental study of the thickness effect to fatigue strength, International Institute of Welding, XIII-2434-12